AGU PUBLICATIONS

JGR

Journal of Geophysical Research: Atmospheres

RESEARCH ARTICLE
10.1002/2016JD025601

Key Points:
- A novel model to assess radiometric calibration impact on Earth measurement of thermal emissive band with application to AVHRR
- Derived errors in AVHRR bands 4 and 5 calibration from the brightness temperature-dependent bias observed during intercomparison with IASI
- Provided algorithm for calibration improvement and bias correction in AVHRR thermal emissive band L1B products

Correspondence to:
T. Chang,
tiejun.chang@ssaihq.com

Citation:
Chang, T., X. Wu, and F. Weng (2017), Modeling thermal emissive bands radiometric calibration impact with application to AVHRR, *J. Geophys. Res. Atmos.*, *122*, 2831–2843, doi:10.1002/2016JD025601.

Received 30 JUN 2016
Accepted 10 FEB 2017
Accepted article online 15 FEB 2017
Published online 3 MAR 2017

Modeling thermal emissive bands radiometric calibration impact with application to AVHRR

Tiejun Chang[1], Xiangqian Wu[2], and Fuzhong Weng[2]

[1]Science Systems and Applications, Inc, Lanham, Maryland, USA, [2]NOAA/NESDIS/STAR, College Park, Maryland, USA

Abstract A novel analytical model of the calibration error impact on the Earth radiance measurement from thermal emissive bands of sensors is developed. The goal is to assess the impact of calibration errors, to evaluate those errors and to perform correction. This model is applied in the correction of bias in Advanced Very High Resolution Radiometer (AVHRR) channels 4 and 5 observed from the intercomparison with Infrared Atmospheric Sounding Interferometer measurements. A two-step regression is used to separate the effects of calibration radiance errors from calibration coefficient errors. In the first step, the calibration radiance error, primarily due to internal calibration target (ICT) imperfections and temperature measurement error, is evaluated using the bias from selected Earth scenes with brightness temperatures close to the ICT temperature. The effects from the ICT imperfections and temperature measurement errors are analyzed collectively. The resulting estimation of the calibration radiance error is 0.30% for channel 4 and 0.33% for channel 5. After correcting the Earth scene radiance for these effects, the errors in the offset and nonlinear coefficient of instrument response are evaluated through the second step of the regression. A weighting function is used to account for the nonuniformity in the data distribution over the Earth radiance range. After the evaluation of the errors, removal of their effects can be achieved either through corrections of the calibration coefficients or correction of the measured radiance. The results are useful for the improvement of the AVHRR IR channel calibration algorithm. This model and two-step regression approach can also be applied to other similar broadband thermal infrared radiometric sensors.

1. Introduction

An intensive calibration assessment is very important for the improvement of sensor calibration. The goal of the model development presented in this paper is to derive the calibration error from a radiance-dependent bias in the Earth measurements for thermal emissive bands. This radiance-dependent bias is usually observed in comparison to a more accurate reference, such as a sensor with high spectral resolution and sufficient spectral coverage. In application to Advanced Very High Resolution Radiometer (AVHRR), we use the Infrared Atmospheric Sounding Interferometer (IASI) as such a reference. The calibration errors are derived, and the AVHRR Earth measurements can subsequently be corrected.

AVHRR is a spectral radiometer that has been measuring reflected solar and emitted thermal radiation from land, sea, clouds, and the atmosphere since 1978. Its third generation (AVHRR/3) has been on board NOAA satellites since 1998 and is also on board the European Organization for Exploitation of Meteorological Satellites (EUMETSAT) polar orbiting operational meteorological satellites (MetOp). MetOp-A, the first in the MetOp series, was launched in October 2006. As a part of the Initial Joint Polar System (IJPS), the National Environmental Satellite, Data, and Information Service (NESDIS) of the National Oceanic and Atmospheric Administration (NOAA) is responsible for the MetOp-A AVHRR calibration. Environmental monitoring, especially climate change detection, requires highly accurate and stable radiance measurements [*Ohring*, 2006]. A prerequisite to realizing the potential of AVHRR data for quantitative applications is accurate instrument calibration.

The infrared (IR) channels on AVHRR are calibrated using an onboard blackbody (BB) with reference to cold space, while the nonlinearity in instrument response was characterized at prelaunch using Thermal Vacuum (TV) test data. The imperfection in the BB emissivity, BB temperature measurement error, and errors in the calibration coefficients impact Earth scene radiance measurement. Assessing the impact of these errors on the retrieved radiance and correcting the resulting bias are essential to enhance product accuracy. This paper focuses on modeling the impact of these errors on Earth scene radiance measurements for the AVHRR IR channels and correcting the calibration coefficients. This model, combined with the

intercomparison to a reference sensor, provides feasibility for regression of the calibration errors and correction of the calibration coefficients. A two-step regression approach is proposed to separate the impact from errors in calibration radiance from those in the calibration coefficients. The intercomparison approach ensures high-quality and intercalibrated measurements from the international constellation of operational satellites [*Goldberg et al*., 2011]. In this work, we use measurements from IASI as reference. IASI is a sensor with high spectral resolution, broad spectral coverage, high accuracy, and excellent stability [*Aumann and Pagano*, 2008, *Blumstein et al*., 2004, 2007; *Larar et al*., 2010; *Hewison et al*., 2013]. In addition, the MetOp-A payload includes both IASI and AVHRR instruments, ensuring an abundance of collocated measurements that enhances the accuracy of the intercomparison and regression results. Recent studies comparing MetOp-A AVHRR and IASI have shown an Earth scene brightness temperature (BT)-dependent bias in the AVHRR infrared thermal channel radiance products [*Wang and Cao*, 2008; *Mittaz and Harris*, 2011; *Madd et al*., 2011; *Wang et al*., 2015].

Mittaz and Harris performed an analysis of the AVHRR prelaunch characterization and reprocessed the radiance using a count-based quadratic algorithm [*Mittaz and Harris*, 2011]. Their correction of the AVHRR bias using the reprocessed radiance was performed by adjusting the parameters to minimize the bias using adjustable offsets (an offset for calibration and an offset for Earth scene retrieval) and onboard BB emissivity. Their work provides very valuable reference for assessing the AVHRR calibration algorithm. However, the use of two offsets in the Mittaz and Harris paper causes ambiguity in the regression and may be unnecessary as the effects from the two offsets are similar. In addition, the nonlinear coefficient correction and the reflectance of Earth radiance off of BB are not considered in their model. The investigation in this paper focuses on the development of a physical model to assess and correct calibration errors arising from the calibration radiance, the calibration offset, and the nonlinear coefficient. The reflection off of BB has also been considered in the model. This model can also be used to assess the calibration bias impact on Earth radiance measurement. The BT-dependent bias is used as an input for regression with the model being used to evaluate the calibration errors. Both the calibration coefficient and Earth scene radiance can be corrected using the derived errors.

2. Background

2.1. AVHRR

2.1.1. AVHRR and IR Channel Calibration

The AVHRR on board the MetOp-A has three solar channels in the visible to near-infrared region covering 0.58–0.68, 0.72–1.10, and 1.58–1.64 μm (channels 1, 2, and 3A, respectively), and three thermal infrared channels covering 3.55–3.93, 10.3–11.3, and 11.5–12.5 μm (channels 3B, 4, and 5, respectively). The cross-track scan covers an angular range of ±55.4° with 2048 samples in each scan. The instantaneous field of view is 0.074°, corresponding to 1.1 km spatial coverage at nadir. The channels 4 and 5 detectors are Mercury-Cadmium-Telluride (Hg-Cd-Te), operating in photoconductive (PC) mode, which exhibit nonnegligible nonlinear responses. A great deal of effort has been made to characterize these nonlinearities and to enhance the Earth scene radiance measurement accuracy [*Mittaz and Harris*, 2011; *Mittaz et al*., 2009; *Weinreb et al*., 1990; *Xiong et al*., 2003; *Walton et al*., 1998; *Sullivan*, 1999].

Currently, a radiance-based nonlinear correction algorithm is used for level 1B (L1B) data [*Sullivan*, 1999]. Mittaz and Harris pointed out some issues regarding the radiance-based algorithm and prelaunch nonlinear characterization [*Mittaz and Harris*, 2011; *Mittaz et al*., 2009]. Our investigation also shows correlations and dependencies between the calibration coefficients in the radiance-based nonlinear correction. It is necessary to test an alternative nonlinear correction algorithm. Many radiometric sensors use a count-based quadratic nonlinear correction, especially for IR bands [*Weinreb et al*., 1990; *Xiong et al*., 2003]. To test the count-based quadratic nonlinear correction we present in this paper, MetOp-A AVHRR prelaunch test data are reanalyzed to generate nonlinear correction coefficients and counts in AVHRR L1B data from selected days are reprocessed using the count-based quadratic nonlinear correction, as Mittaz and Harris performed in 2011 [*Mittaz and Harris*, 2011].

2.1.2. AVHRR Data Reprocessing

In prelaunch characterization of instrument response using an external calibration target (ECT) and cold reference at space view (SV), the instrument nonlinear response can be represented as [*Mittaz and Harris*, 2011; *Xiong et al*., 2003]

$$R_{ECT} = a_0 + a_1(C_{SV} - C_{ECT}) + a_2(C_{SV} - C_{ECT})^2 \quad (1)$$

where R_{ECT} is the ECT radiance, C are instrument response to the targets in counts, and a_0, a_1, and a_2 are the offset, linear coefficient, and nonlinear coefficient obtained by fitting equation (1) with a range of R_{ECT}. Postlaunch, the coefficients can change as instrument response changes.

For AVHRR thermal bands, lower radiance corresponds to higher digital count output. The on-orbit calibration using the internal calibration target (ICT) updates the linear coefficient of the response function. With these coefficients, the postlaunch Earth scene radiance can be retrieved from Earth view counts by

$$R_{EV} = a_0 + \frac{R_{ICT} - a_0 - a_2(C_{SV} - C_{ICT})^2}{(C_{SV} - C_{ICT})}(C_{SV} - C_{EV}) + a_2(C_{SV} - C_{EV})^2 \quad (2)$$

where R_{ICT} is the calibration radiance at the ICT view. In the AVHRR L1B products, raw counts and ICT temperatures are provided. Combining these data with the calibration coefficients from prelaunch, the Earth scene radiance can be reprocessed using equation (2).

2.2. Intercomparison of AVHRR With IASI

2.2.1. IASI

IASI, consisting of a Michelson interferometer-based spectrometer and an imaging system, represents a significant advancement in the quality of spectral radiance measurements emitted from the Earth. IASI covers the IR spectra between 645 and 2760 cm^{-1} (3.6–15.5 μm) with a sampling resolution of 0.25 cm^{-1}. IASI's spectral radiance has a full coverage on AVHRR channels 4 and 5, but not channel 3B. The scan angle range is ±48.3° with 30 fields of view (FOV). Within each FOV, a 2 × 2 circular pixel matrix covers approximately 50 km × 50 km at nadir with 12 km × 12 km coverage for each pixel. The IASI spectral radiance is well calibrated using an onboard BB and a cold deep space reference. The onboard BB temperature is around 293 K. The temperature and radiative environment effects on the onboard BB, the scan mirror reflectivity variation, and scan mirror emission are considered in the on-orbit calibration and Earth scene spectral radiance measurements.

A number of investigations have demonstrated that IASI has been operated well within its specifications for both spectral and radiometric calibration accuracy [*Aumann and Pagano*, 2008; *Blumstein et al*., 2004, 2007; *Larar et al*., 2010]. These studies demonstrated that the accuracy and stability of IASI measurements are within 0.1 K. Accurate and stable measurements of Earth scene spectral radiances with high spectral resolution makes IASI ideal as a reference for intercomparison and intercalibration. Both AVHRR and IASI are on board the MetOp-A satellite. This eliminates many uncertainties in intercalibration due to mismatch in time and viewing geometry. Numerous collocated measurements covering various Earth scenes on different seasons offer a great advantage for intercomparison between these two sensors.

There are still certain uncertainty and bias in IASI measurement that impact on the comparison and the modeling results. The impact depends on the changes in the IASI calibration algorithm and calibration coefficients. IASI measurement can be a radiometric reference for AVHRR as long as it provides more accurate and stable measurement than AVHRR. This paper focuses on model development and utilizes AVHRR and IASI intercomparison for the demonstration. If the accuracy of IASI measurements is improved in the future, the present modeling accuracy can also be enhanced. This modeling can also be a useful tool for future MetOp-C calibration verification.

2.2.2. Spectral and Collocation Processing

In order to compare AVHRR band-averaged radiances with IASI spectral radiances, two necessary data processes should be performed: convolving the IASI data spectrally to match the AVHRR spectral response function (SRF) and retrieving the AVHRR data spatially to match the IASI spatial response function. The IASI level 1c (L1c) radiance product provides an IR-integrated imager for each IASI FOV, which is derived from the coregistered AVHRR pixel radiance. This contains radiances for two AVHRR channels (channels 4 and 5) [*Phillips and Schlüssel*, 2005]. We define this AVHRR radiance as AVHRR radiance in IASI L1c. The processing algorithm of AVHRR radiance in IASI L1c uses radiance clusters along with associated weighting values and standard deviations to account for the Earth scene inhomogeneity [*Phillips and Schlüssel*, 2005]. These products are convenient for comparing IASI and AVHRR radiance from the current operational calibration algorithm. However, this is insufficient since the evaluation of an alternative calibration algorithm requires the calibrator data and raw counts from the AVHRR measurements [*Mittaz and Harris*, 2011]. Another

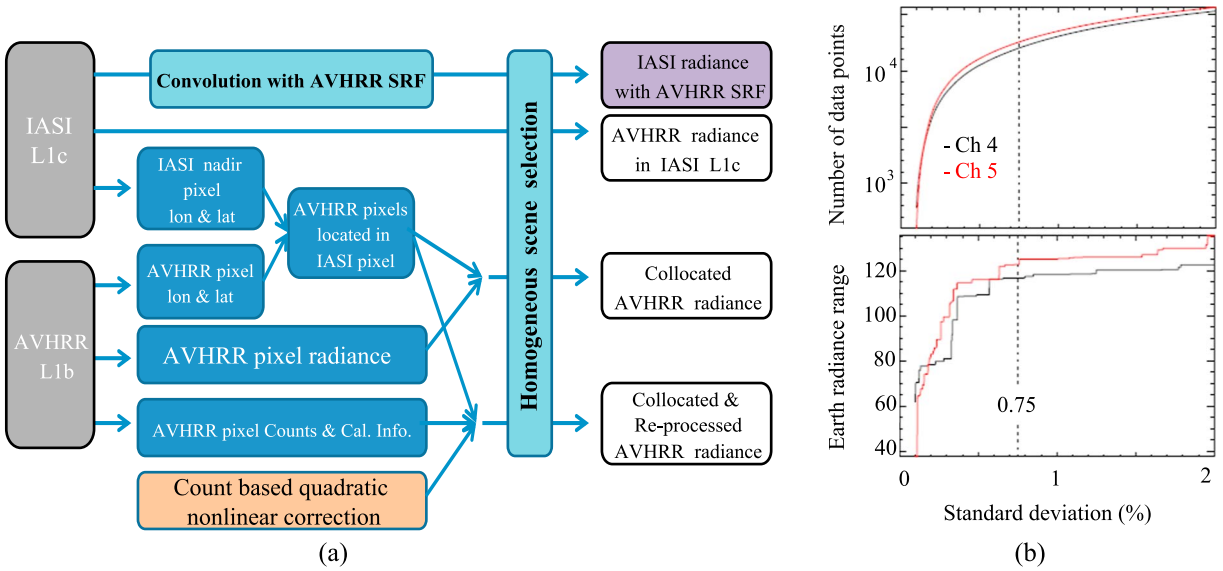

Figure 1. (a) Illustration of radiance processing for comparison. (b) Illustration of the determination of the standard deviation threshold based on the number of data points and the Earth scene radiance range. The standard deviation is calculated in percentage for the radiance variation from the average of the selected pixels in a FOV.

approach is to extract the collocated AVHRR radiance within the IASI FOV from the AVHRR L1B product through postprocessing, similar to that used in reference [*Mittaz and Harris*, 2011]. Since the IASI FOV at nadir covers a 12 km footprint while an AVHRR pixel covers a 1.1 km footprint, the AVHRR pixels inside the IASI FOV should be averaged to produce collocated radiance comparable to IASI radiance. Approximately 130 AVHRR pixels for each IASI FOV are selected based on the distance between their centers. The standard deviation of the radiance of the selected pixels represents scene homogeneity. The advantage of using this collocation method is the availability of calibration data and raw counts in AVHRR L1B product, which is essential for reprocessing the data using the count-based nonlinear correction algorithm described in section 3.1.

The chart in Figure 1a illustrates the processing flow for IASI radiance corresponding to an AVHRR channel, AVHRR radiance in IASI L1c, collocated AVHRR radiance, and collocated and reprocessed AVHRR radiance. Since the focus of this work is on radiometric calibration evaluation and correction, the collocated pixels at nadir, the fourteenth and fifteenth FOV, are used for the comparison to avoid effects from the response versus scan angle (RVS).

The accuracy of the comparison depends on the scene homogeneity, especially for the collocated radiance. Similar to the homogenous scene selection criteria in the work by Mittaz and Harris, the standard deviation of AVHRR pixels collocated in an IASI FOV is used as an indicator of the homogeneity of that FOV [*Mittaz and Harris*, 2011]. The homogenous scene selection criteria considers the homogeneity-associated noise level indicated by the standard deviation, the number of data points, and the Earth radiance range, which is defined as the difference between the maximum and minimum radiance for the selected collocated data. Figure 1b shows the number of data points and Earth radiance range as a function of the standard deviation, which is calculated in percentage for the radiance variation from the average of the selected pixels in a FOV. A threshold of 0.75% is applied for the homogenous scene selection.

3. Calibration Error Impact Model

3.1. Calibration Radiance Error Model

To identify the major systematic error source of the AVHRR radiance bias, a model to assess the impact of the onboard calibration radiance error and calibration coefficient error is necessary. It is known that the ICT is not a perfect BB. In the AVHRR operational calibration, the ICT radiance is calculated with an assumed emissivity of 1 despite the fact that this is among the major causes of bias in the observations. These effects include not only an ICT radiation reduction but also reflections of the instrument and Earth scene radiance off of the ICT.

The AVHRR ICT is at instrument ambient temperature, so that reflections of the instrument radiance partially compensate for ICT radiance reduction. Thus, ICT BB imperfection effects on the Earth measurement bias are related to the thermal environment. Considering these major systematic error effects, the calibration radiance at ICT view becomes

$$R_{\mathrm{ICT}} = \varepsilon_{\mathrm{ICT}} B(T_{\mathrm{ICT}}) + f_{\mathrm{inst}}(1-\varepsilon_{\mathrm{ICT}}) B(T_{\mathrm{inst}}) + f_{\mathrm{EV}}(1-\varepsilon_{\mathrm{ICT}}) R_{\mathrm{EV}} + f_{\mathrm{SV}}(1-\varepsilon_{\mathrm{ICT}}) R_{\mathrm{SV}} \tag{3}$$

where $\varepsilon_{\mathrm{ICT}}$ is the ICT emissivity, f_{inst}, f_{EV}, and f_{SV} are the source factors associated with the reflection off of the ICT from instrument radiance R_{inst}, Earth radiance R_{EV}, and deep space radiance R_{SV}, respectively. Due to the zero radiance from deep space $R_{\mathrm{SV}} = 0$, its reflection off of the BB $f_{\mathrm{SV}}(1-\varepsilon_{\mathrm{ICT}})R_{\mathrm{SV}}$ is also zero. The source factors represent the ratio of the solid angle covered by these radiance sources to the BB hemisphere (assuming the BB is a Lambertian reflector), and we have $f_{inst} + f_{\mathrm{EV}} + f_{\mathrm{SV}} = 1$. Therefore, the constraint $f_{inst} + f_{\mathrm{EV}} < 1$ is applied to equation (3). Here $B(T)$ is the BB radiance at temperature T calculated using the Planck equation for consistency with traditional expressions in the calibration algorithm. Since the ICT is at instrument ambient temperature, the ICT temperature is used to represent the instrument temperature for convenience $B(T_{inst}) = B(T_{\mathrm{ICT}})$. The temperature variation among parts of the instrument is small, and its effect on the second term of equation (3) is expected to be insignificant.

Besides the error caused by ICT BB imperfections, another error source is the ICT temperature measurement, which includes the PRT temperature measurement error, the temperature difference between the embedded PRT and the BB surface, and the effect of BB temperature nonuniformity. These temperature measurement errors can cause systematic bias and random noise on the calculated ICT radiance. The systematic error is difficult to separate from the BB imperfection effect, and these two effects will be analyzed collectively. The relative error in calibration radiance can be derived from equation (3) with an extra term from the BB temperature measurement error effect,

$$\frac{\Delta R_{\mathrm{ICT}}}{R_{\mathrm{ICT\_L1B}}} = (1 - f_{\mathrm{inst}} - f_{\mathrm{EV}})(1-\varepsilon_{\mathrm{ICT}}) - \frac{1}{R_{\mathrm{ICT\_L1B}}}\left(\frac{\mathrm{d}B(T)}{\mathrm{d}T}\right)_{T=T_{\mathrm{ICT}}} \Delta T_{\mathrm{ICT}} + f_{\mathrm{EV}}(1-\varepsilon_{\mathrm{ICT}})\frac{R_{\mathrm{ICT\_L1B}} - R_{\mathrm{EV}}}{R_{\mathrm{ICT\_L1B}}} \tag{4}$$

where $\Delta R_{\mathrm{ICT}} = R_{\mathrm{ICT\_L1B}} - R_{\mathrm{ICT}}$ is the difference between the calibration radiance used in current L1B calibration algorithm ($R_{\mathrm{ICT\_L1B}} = B(T_{\mathrm{ICT}})$) and that from equation (3). The error for a measurement is defined as the difference between the measured value X and the true value X_{true}, $\Delta X = X - X_{true}$. The third term on the right-hand side of equation (4) depends on the difference between the Earth scene and ICT radiances. The first two terms, representing the ICT BB imperfection effect and ICT systematic temperature measurement error, are independent of the Earth scene. These two terms can be grouped together as an effective emissivity error, which is defined as

$$\Delta\varepsilon_{\mathrm{ICT}}^{(\mathrm{eff})} = \left(\frac{\Delta R_{\mathrm{ICT}}}{B(T_{\mathrm{ICT}})}\right)_{R_{\mathrm{EV}}=R_{\mathrm{ICT\_L1B}}} = (1 - f_{\mathrm{inst}} - f_{\mathrm{EV}})(1-\varepsilon_{\mathrm{ICT}}) - \frac{1}{R_{\mathrm{ICT\_L1B}}}\left(\frac{\mathrm{d}B(T)}{\mathrm{d}T}\right)_{T=T_{\mathrm{ICT}}} \Delta T_{\mathrm{ICT}} \tag{5}$$

The reflections of the instrument radiance and Earth scene radiance partially compensate the reduction of ICT radiance. It is thus expected that the first term in the equation for the effective emissivity error should be less than $1 - \varepsilon_{\mathrm{ICT}}$.

The SRF error impact on radiance bias has been discussed in the work by Mittaz and Harris for AVHRR [*Mittaz and Harris*, 2011]. The sensitivity to the SRF error depends on the spectral features of the Earth observation. Unlike a sounding instrument, AVHRR channels 4 and 5 are IR window channels, in which the biases are less sensitive to the SRF error.

3.2. Calibration Coefficient Error Model

As pointed out in section 2.1.1, the current operational nonlinear correction algorithm has some issues with the correlation and dependency between the calibration coefficients. These issues make the assessment of the calibration error impact difficult. The effect of calibration coefficient error is analyzed using the count-based quadratic nonlinear algorithm. The impact of calibration error on the Earth scene radiance can be derived from equation (2), using a perturbation method $\frac{\Delta R_{\mathrm{EV}}}{R_{\mathrm{EV}}} = \frac{R_{\mathrm{EV}}(R_{\mathrm{ICT}}, a_0+\Delta a_0, a_2+\Delta a_2) - R_{\mathrm{EV}}(R_{\mathrm{ICT\_L1B}}, a_0, a_2)}{R_{\mathrm{EV}}(R_{\mathrm{ICT\_L1B}}, a_0, a_2)}$, where Δa_0 is the error in instrument response offset and Δa_2 is the error in instrument response nonlinearity. After combining this with the calibration error $\frac{\Delta R_{\mathrm{ICT}}}{R_{\mathrm{ICT\_L1B}}}$ derived in the previous section and applying the first-order approximation, the induced relative error in radiance can be expressed as

$$\frac{\Delta R_{EV}}{R_{EV}} \approx \Delta\varepsilon_{ICT}^{(eff)} + \left(\frac{1}{R_{EV}} - \frac{1}{R_{ICT\_L1B}}\right)\Delta a_0 + \frac{(R_{EV} - R_{ICT\_L1B})}{{a_1}^2}\Delta a_2^{(eff)} \quad (6)$$

with $\Delta a_2^{(eff)} = \left(\Delta a_2 - \frac{{a_1}^2 |d\varepsilon_{ICT}| f_{EV}}{R_{ICT\_L1B}}\right)$. The expression $da_2^{(eff)}$ comes from two sources; the error in instrument response nonlinearity and the effect induced by the reflection of the Earth scene radiance off of the imperfect ICT BB. On orbit, the errors induced by these two effects cannot be separated and are treated effectively as one error which is proportional to the difference between the Earth scene radiance and the ICT radiance. AVHRR is calibrated scan by scan. The instrument self-emission variation from space view to Earth view is very small and does not contribute with a systematic error. The space view contamination effects are more complicated. If the space view contamination is continuous, the contaminations can be treated as a combination of two effects; the average difference between the prelaunch test and on-orbit calibration, which can be handled by the error in offset and random noise caused by the fluctuations around the average.

3.3. Two-Step Regression

The terms on the right-hand side of equation (6) have a different dependency on Earth scene radiance. The effective emissivity error term is independent of Earth scene radiance, the da_0 term is proportional to $\left(\frac{1}{R_{EV}} - \frac{1}{R_{ICT\_L1B}}\right)$, and the $\Delta a_2^{(eff)}$ term is proportional to $\frac{(R_{EV} - R_{ICT\_L1B})}{{a_1}^2}$. These dependencies make it possible to analyze the bias through regression. In this work, a two-step regression is applied to reduce the effects of correlation between difference error sources. The first step is to evaluate the effective emissivity error using the bias from the scenes with radiance close to that of the ICT. For those scenes, the second and third terms in equation (6) are negligible and the average of the bias is the effective emissivity error, $\Delta\varepsilon_{ICT}^{(eff)} = \left(\frac{\Delta R_{EV}}{R_{EV}}\right)_{R_{EV}=R_{ICT\_L1B}}$. After the effective emissivity error is corrected, a regression analysis of the bias over a broad range of Earth scene BTs provides an evaluation of errors in the calibration coefficients. In the second regression step, the Earth scene radiance range and bias data radiance distribution affect the results. A sufficiently large radiance range reduces the correlation between the offset error effect and nonlinearity error effect. The problem caused by a nonuniform radiance distribution of the bias data can be solved by introducing a weighting function that is described in the appendix.

4. Regression and Correction

4.1. Earth Scene BT-Dependent Bias

The relative radiance difference between AVHRR and IASI for channel 4 is shown in Figure 2, where Figure 2a is the comparison using AVHRR radiance in IASI L1c and Figure 2b is using collocated AVHRR L1B radiance. The bias is from −1% to 0.5%, and the Earth scene BT dependence is similar with those of previous work [*Wang and Cao*, 2008; *Mittaz and Harris*, 2011]. The plots are from 1 day observations, and the Earth scene BT range can be different within that day (1/12/2011). The difference between biases from AVHRR radiance in IASI L1c and collocated radiances is plotted in Figure 2c, which illustrates the collocated radiance match-up difference. The mean is very close to 0 and the standard deviation is 0.04% for both channels 4 and 5. The differences are due to the algorithm difference and collocation processing, which can induce noise in the radiances. It is more meaningful to compare the fitting of the two biases using a given model over the entire Earth scene. Figure 2d shows the two fitting curves using a quadratic function. The fitting uncertainties, calculated from the fitting residues, are both 0.1%. Figure 2 shows the results for channel 4, and channel 5 has a similar Earth scene-dependent biases and processing uncertainties. The reprocessed radiance using the count-based nonlinear correction also shows a similar Earth scene dependent bias. Note that as the coefficients for both the radiance-based nonlinear correction and the count-based correction are based on prelaunch test data, the errors from the prelaunch characterization are propagated to the operational radiance [*Mittaz and Harris*, 2011]. In addition, the problems with the operational calibration equations discussed in a paper by *Mittaz et al*. [2009] also increase the uncertainty in the radiance product. The bias is relatively large for cold scenes in both channels. As shown in equation (6), the second term is the offset effect and is proportional to $\left(\frac{1}{R_{EV}} - \frac{1}{R_{ICT\_L1B}}\right)$. The offset error is dominant for cold scene. For a given offset error, this term changes radically as the radiance decreases and the offset error is magnified for cold scenes. On the other

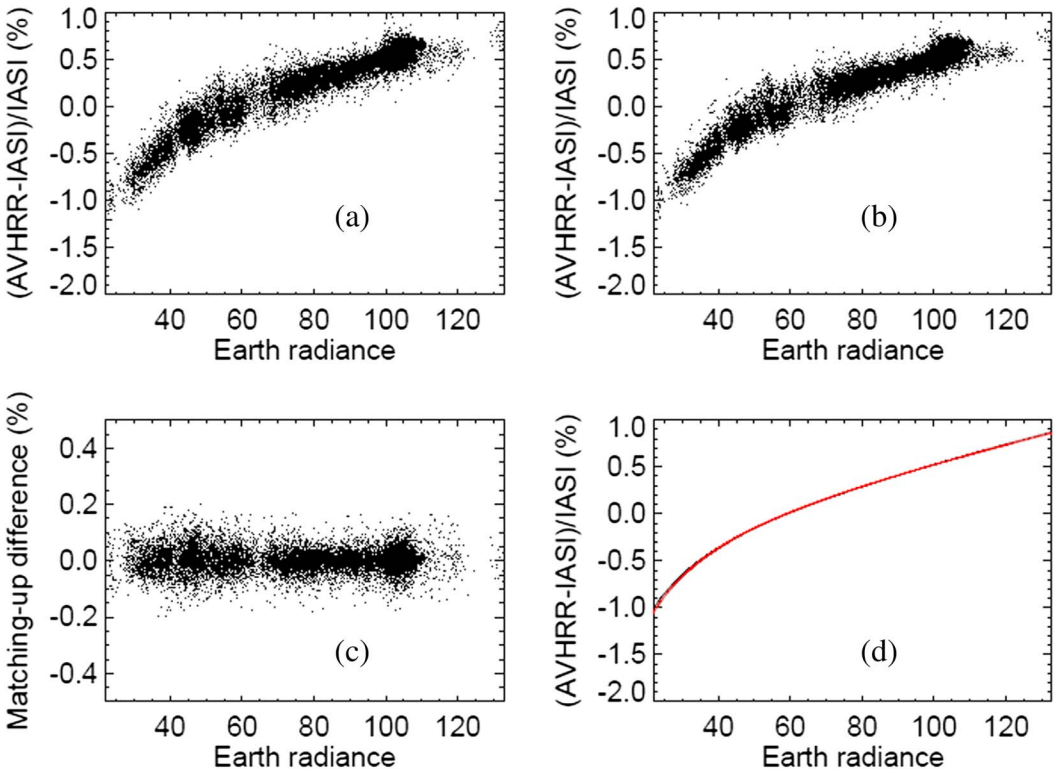

Figure 2. (a) The relative radiance difference between AVHRR and IASI for AVHRR channel 4 versus the Earth scene radiance from the AVHRR radiance in IASI L1c. (b) The difference using the collocated radiance. (c) Relative difference between the bias using the AVHRR radiance in IASI L1c and using the collocated radiance. (d) Quadratic fits of the biases in Figures 2a and 2b are overlapped. The fitting uncertainties, calculated from the fitting residues, are both 0.1%. The data are selected from homogeneous Earth scene on day 1/12/2011. The radiance values are presented in units of mW/m^2 sr cm^{-1}.

hand, the large amount of samples with radical radiance dependence over cold scene can increase the regression accuracy for the offset error (in section 4.2.2).

4.2. Two-Step Regression

The bias in the reprocessed radiance is analyzed using the model presented in section 3.1 for the count-based nonlinear correction. A two-step regression analysis is performed to evaluate the calibration radiance error and the calibration coefficient error. After the errors are obtained from the regressions, the Earth scene radiance can be corrected.

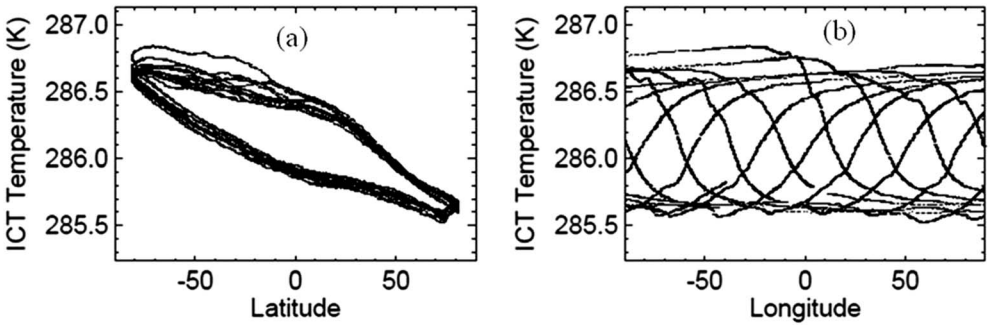

Figure 3. The ICT temperature fluctuates in the orbital frequency. (a) ICT temperature as a function of latitude. (b) ICT temperature as a function of longitude. The data are selected after applying the homogeneity filter described in section 2.2.2. Since the variation repeats with orbit, the plot in Figure 3b is for selected longitude range from −90° to 90°.

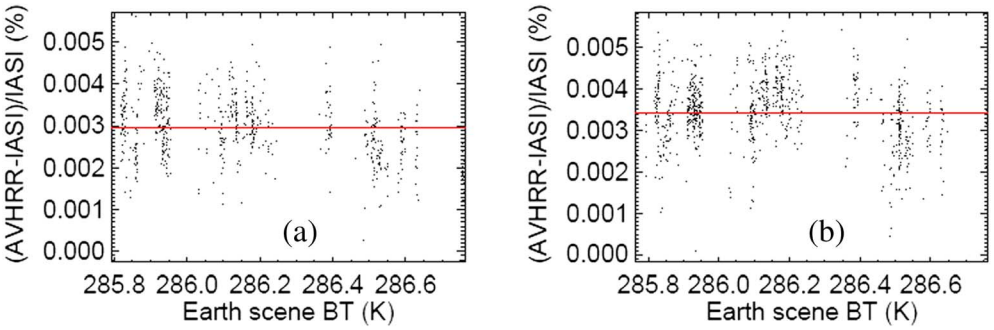

Figure 4. Effective emissivity error evaluated from the selected radiance versus Earth scene BT, (a) for channel 4 and (b) for channel 5. The lines are the averaged effective emissivity error. The data are selected from 1/12/2011.

4.2.1. Step 1: Regression for Calibration Radiance Error

The ICT temperature fluctuates in the orbital frequency [*Steyn-Ross and Steyn-Ross*, 1992]. The range of the ICT temperature variation is approximately 1 K, as shown in Figure 3. ICT temperatures for corresponding scans are recorded in the AVHRR L1B data, which are associated to each IASI FOV. The ICT radiance calculated from the ICT temperature is used to select scenes with Earth scene radiance within 2% of the ICT radiance ($\left|\frac{R_{EV}-R_{ICT\_L1B}}{R_{EV}}\right| < 0.02$).

The averaged relative bias of the selected Earth scenes is used to evaluate the ICT effective emissivity error using $\Delta\varepsilon_{ICT}^{(eff)} = \left(\frac{\Delta R_{EV}}{R_{EV}}\right)_{R_{EV}=R_{ICT\_L1B}}$, as shown in Figure 4. The effective emissivity error is averaged using data from the year 2011 (1 day each month), and the number of data points selected in each day is used to weight the average and associated standard deviation. The effective emissivity error is 0.0030 ± 0.0001 for channel 4 and 0.0033 ± 0.0002 for channel 5. The reason for performing the evaluation using data from different days in a year is to verify consistency and to remove any seasonal fluctuations. Evaluation accuracy can be enhanced by increasing the amount of data analyzed.

4.2.2. Step 2: Regression for Calibration Coefficient Error

After the calibration error is evaluated and its impact is removed from the bias, the second regression step is performed to assess the calibration coefficient errors. If no proper method is applied, the fit results depend on the Earth radiance range, number of points, and the data distribution. The distribution is not uniform with Earth scene radiance, as shown in Figure 5 and varies with time as well. The regression analysis requires not only a sufficient number of data points but also a large range within those data points. To make the contribution from different radiance ranges uniform in the regression, a weighting function is applied to each data point, which is derived from the data distribution, $W_i = \frac{1}{C_{R_i-0.5}^{R_i+0.5}}$, where $C_{R_i-0.5}^{R_i+0.5}$ is the number of data points within a 1 mW/m^2 sr cm^{-1} range centered at R_i (see Appendix A). An in-house regression code has been

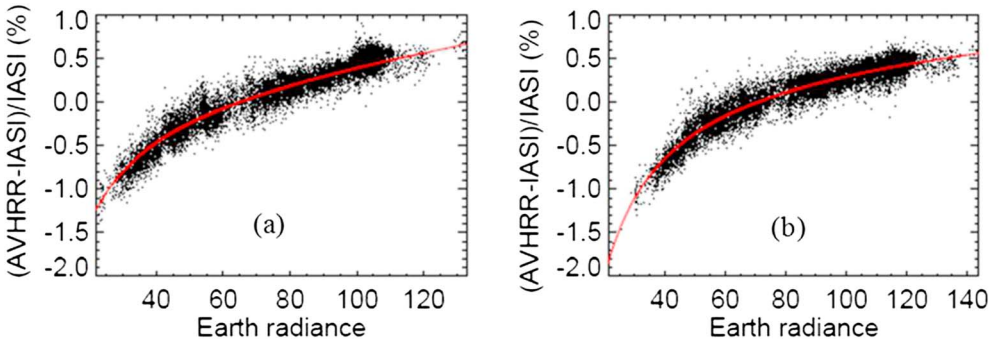

Figure 5. Scene temperature-dependent bias analysis (a) for channel 4 and (b) for channel 5. The bias curves after the effective emissivity error correction are fit using the second and third terms of equation (6). The data are selected from collocated radiance on 1/12/2011. The radiance values are presented in units of mW/m^2 sr cm^{-1}.

Table 1. The Effective Emissivity Error, Offset Error Δa_0, and Effective Nonlinearity Error $\Delta a_2^{(eff)}$ Averaged From the Regression Analysis on Different Days in Year 2011[a]

	Channel 4	Channel 5
$\Delta\varepsilon_{ICT}^{(eff)}$	0.0030	0.0033
$\Delta\varepsilon_{ICT}^{(eff)}$ uncertainty	0.0001	0.0002
a_0	0.972	0.636
Δa_0	−0.353	−0.532
Δa_0 uncertainty	0.003	0.003
Corrected a_0	1.325	1.168
a_2	1.84×10^{-5}	1.18×10^{-5}
$\Delta a_2^{(eff)}$	0.17×10^{-5}	0.08×10^{-5}
$\Delta a_2^{(eff)}$ uncertainty	0.08×10^{-5}	0.06×10^{-5}
Corrected a_2	1.67×10^{-5}	1.10×10^{-5}

[a]The uncertainties of coefficient corrections are estimated from the regression. The coefficients a_0 and a_2 are derived from the analysis of prelaunch test data. The coefficient a_0 has units of mW/m^2 sr cm^{-1} and a_2 has units of mW/m^2 sr cm^{-1}/*count*^{2}.

developed to perform the regression with this weighting function. Figure 5 shows the fitting results using equation (6) for the Earth scene radiance bias after the effective emissivity error correction, where the lines represent the fits using the model. The errors in calibration coefficients Δa_0 and $\Delta a_2^{(eff)}$ are determined from the regression.

4.3. Corrections and Assessments

4.3.1. Calibration and Bias Corrections

After the calibration errors are evaluated from the two-step regression, the corrections of the calibration coefficients and Earth scene radiance are performed. The evaluation of calibration coefficient errors using data from different days of a year can reduce random noise that is composed of both noises in the radiance measurements and in the approximation of a homogeneous Earth scene. Table 1 lists the averaged calibration coefficient error and the uncertainties derived using the intercomparison from the year 2011 (day 1 of each month). As shown in Figure 5, the bias at cold scenes is magnified. The radiance dependence and large number of samples at low radiance range can reduce the regression uncertainty for the offset error. On the other hand, the effect of nonlinear coefficient error is relatively small for the high radiance range.

The calibration correction is used for the correction of the retrieved Earth scene radiance. With the error defined as $X_{true} = X - \Delta X$, the corrected Earth scene radiance is

$$R_{EV}^{(corrected)} = R_{EV} - \Delta R_{EV} = R_{EV} - \Delta\varepsilon_{ICT}^{(eff)} R_{EV} - R_{EV}\left(\frac{1}{R_{EV}} - \frac{1}{R_{ICT\_L1B}}\right)\Delta a_0 - R_{EV}\frac{(R_{EV} - R_{ICT\_L1B})}{{a_1}^2}\Delta a_2^{(eff)} \quad (7)$$

Figures 6a and 6b show the difference between IASI and AVHRR after the corrections, for channels 4 and 5, respectively. The distributions of the bias in BT before and after the error corrections, for both channels, are shown in Figures 6c and 6d, respectively. After correction, the AVHRR-IASI difference and the Earth scene BT dependence are reduced significantly. The standard deviation of the radiance difference is 0.1% for both channels, and the residual difference has a distribution close to Gaussian, which indicates that the differences are mainly due to the random noise. However, the dependence is still noticeable, which suggests that the regression approach adopted here may not be optimal over the full dynamic range. For comparison, the matching-up difference in Figure 2c are due to random noise while Figure 6 shows a slight radiance dependence. A further model improvement for sensor-specific considerations may be necessary.

4.3.2. Correction for AVHRR Operational Radiance Product

The current AVHRR operational radiance is a product that uses a radiance-based nonlinear correction. The calibration radiance error, the change in offset from prelaunch test to on-orbit operation, and the error in the nonlinearity characterization result in a bias in the L1B operational radiance product. Developing an error impact model from the radiance-based nonlinear algorithm is very challenging due to the calibration

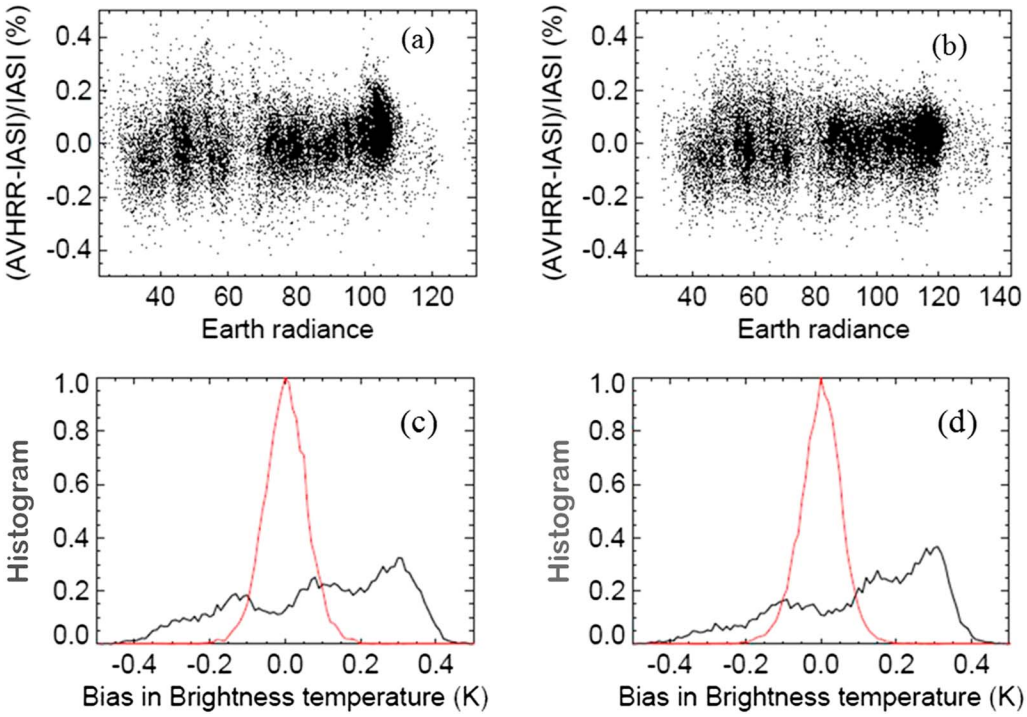

Figure 6. The AVHRR and IASI difference after the correction, (a) for channel 4 and (b) for channel 5. The distribution of the bias in BT before (black curves) and after (red curves) corrections, (c) for channel 4 and (d) for channel 5. The distribution is normalized to the maximum counts in a bin. The data are selected from 1/12/2011. The radiance values in Figures 6a and 6b are presented in units of mW/m^2 sr cm^{-1}.

algorithm issues. However, since there are similar error effects for the operational radiance product and reprocessed radiance, the same error impact model (equation (6)) and radiance correction (equation (7)) can also be applied for the L1B radiance correction.

After the Earth scene BT-dependent bias is determined from the AVHRR-IASI comparison, a similar two-step process to the one discussed in section 4.3.1 can also be applied. The first step is to evaluate the calibration radiance error from the bias of the Earth scenes with BT close to the ICT temperature. The second step is to perform the regression for determining the offset error and the effective nonlinear coefficient error using the error impact model (equation (6)). The radiance correction can be applied using equation (7). The errors evaluated in the analysis can also be used for calibration algorithm assessment. With this procedure, a user can perform the correction to radiance with coefficient errors for a given period of time and the reprocessing is not required.

4.3.3. Calibration Error Impact Assessment

The AVHRR bias is essentially composed of the calibration radiance error and calibration coefficient errors. These errors may not be introduced solely by the prelaunch characterization and the issues of the radiance-based nonlinear correction algorithm. Some are related to the environmental and operational differences between the prelaunch thermal vacuum (TV) test and on-orbit calibration. For example, the offset error may be caused by changes in instrument response and contamination of the onboard calibrators; the ICT calibration radiance error is related to not only the ICT emissivity but also the thermal environment around the ICT, which is different between the prelaunch TV testing and postlaunch operations. The ICT BB imperfection certainly has an effect on the calibration radiance, even though it is partially compensated by the reflections. The bias in ICT temperature measurement also contributes to calibration radiance error and, however, the effect of random noise in the temperature measurement is insignificant after the average in the regression for calibration radiance error.

The calibration error impact on Earth scene radiance measurement can be evaluated [*Chang and Xiong*, 2011]. Figure 7 shows the error effects from the calibration radiance $\Delta\varepsilon_{ICT}^{(eff)}$, offset Δa_0, and nonlinearity $\Delta a_2^{(eff)}$ over the BT range of the Earth measurements from 1/12/2011. The effect of calibration radiance error impacts the entire temperature range and increases with temperature. There is no error effect at

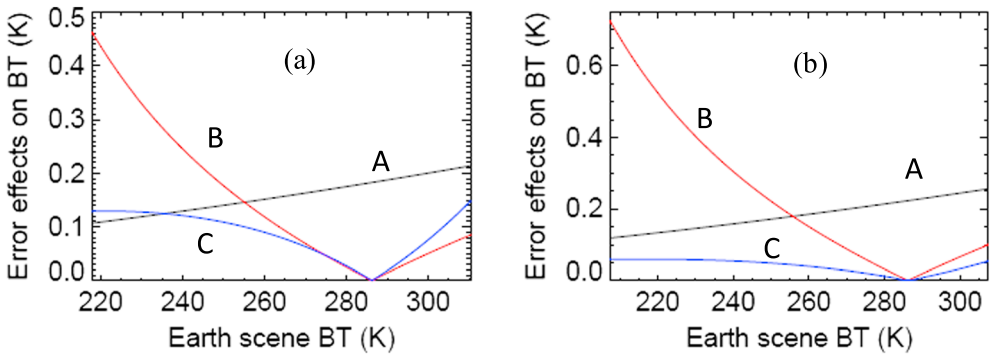

Figure 7. The error effects on temperature versus Earth scene BT, (a) for channel 4 and (b) for channel 5. Curve A is the contribution from calibration radiance error $\Delta\varepsilon_{\mathrm{ICT}}^{(eff)}$, curve B is the contribution from the offset error Δa_0, and curve C is the contribution from nonlinearity error $\Delta a_2^{(eff)}$.

the ICT temperature induced by the errors in calibration coefficients, which is expected. Since the error effect is defined as a positive value, the turning point at the ICT temperature is caused by the sign change of the induced error. The offset error has a greater effect in the lower temperature range. The uncertainty in error derived from the regression analysis of the bias depends on the range of the Earth scene BTs.

Separation of the contributions of offset error and that of nonlinearity error requires a broad range of Earth scene BTs. As shown in Figure 7, the contributions of offset error and nonlinearity error have a certain degree correlation, especially around the ICT temperature and the correlation can cause ambiguity in a regression with a limited sample range. As a result, these two contributions can partially compensate for each other. The calibration algorithm assessment and calibration improvement require that these effects be analyzed separately. For the Earth scenes with very low and very high BTs, the effects of the errors in offset and in nonlinearity are different. The separation of the error contributions can be enhanced by selecting measurement data with more data points and with larger Earth scene BT range, and by applying the proper regression approach.

5. Summary

In this paper, an analytical model of the calibration error impact on Earth radiance measurement is developed, which includes the impacts from calibration radiance error and calibration coefficient error. This model has been applied to the AVHRR Earth scene BT-dependent bias derived from intercomparison with IASI. The AVHRR data from selected days are reprocessed using a count-based quadratic calibration algorithm. The reprocessed radiance is used for testing the calibration algorithm and assessing the impact of the errors in the offset and nonlinearity of the instrument response. The calibration radiance error is primarily due to the ICT BB imperfection and ICT temperature measurement error and these effects are analyzed collectively. The errors in calibration coefficients are primarily due to the prelaunch calibration errors and the environmental difference between prelaunch TV testing and on-orbit operations. This investigation focuses on the error impact model development and determinations of the calibration errors using the model. A two-step regression analysis is proposed and applied to separate the effect from calibration radiance error from those of calibration coefficient errors. In the first step, the calibration radiance error is evaluated using the biases from the selected Earth scenes with BTs close to the ICT temperature. It is found that the calibration radiance error is 0.30% for channel 4 and 0.33% for channel 5. After removing the effects of the errors in calibration radiance from the bias, what remains is mostly caused by the effects of errors in the calibration coefficients, which are investigated in the second regression step. A weighting function is used to account for the nonuniform distribution of data over the Earth scene radiance range. The errors in offset and nonlinearity are evaluated through the regression. The removal of the effects of these errors can be achieved, either through corrections of the radiance or the calibration coefficients. This significantly improves the AVHRR calibration and subsequent operational radiance products. The results in this study are useful for improvement of the AVHRR IR channel calibration algorithm.

This paper focuses on model development and the demonstration for AVHRR using the radiance dependent bias from AVHRR and IASI intercomparison. In this demonstration, the IASI measurement accuracy can impact

on the modeling results, and improvement in the IASI calibration algorithm can enhance the modeling accuracy. This model and method are useful for future MetOp-C AVHRR verification. The calibration error impact model and the two-step regression approach are also useful for vicarious calibration and intercomparison. The model developed in this study can also be applied to other similar thermal infrared broadband radiometric sensors if their radiance-dependent bias in measurements can be assessed using an appropriate reference.

Appendix A: Weighting Function in Regression

The regression accuracy for the calibration coefficient error using equation (6) depends on the Earth radiance range, number of points, and data distribution. A weighting factor from the data in certain radiance range can be used. After testing, we concluded that a 1 mW/m^2 sr cm^{-1} radiance range is appropriate for these two channels and also convenient for computation. The merit function for least squares optimization is defined as [*Press et al*., 1992]

$$\chi^2 = \sum_n \frac{1}{\sigma_n^2}\left[y_n - f(R_n, \Delta a_0, \Delta a_2)\right]^2 \tag{A1}$$

where the sum is over every unit radiance, $y_n = \frac{1}{C_{R_n-0.5}^{R_n+0.5}} \sum_{R_n-0.5}^{R_n+0.5} \frac{\Delta R}{R}$ is the averaged bias in the nth unit radiance range, and $C_{R_n-0.5}^{R_n+0.5}$ is the number of data points in that range centered at R_n. The σ_n is the uncertainty associated with the averaged bias at that unit radiance and for normal distributions, $\sigma_n^2 = \frac{1}{C_{R_n-0.5}^{R_n+0.5}}$. The expression $f(R_n, \Delta a_0, \Delta a_2) = \frac{1}{C_{R_n-0.5}^{R_n+0.5}} \sum_{R_n-0.5}^{R_n+0.5} f(R, \Delta a_0, \Delta a_2)$ is the average in the nth unit radiance range of the right-hand side of equation (6). Converting equation (A1) to the sum over data points, one can have

$$\chi^2 = \sum_i \frac{1}{C_{R_i-0.5}^{R_i+0.5}}\left[y_i - f(R_i, \Delta a_0, \Delta a_2)\right]^2 \tag{A2}$$

where $C_{R_i-0.5}^{R_i+0.5}$ is the number of data points within a unit radiance range centered at R_i, and $W_i = \frac{1}{C_{R_i-0.5}^{R_i+0.5}}$ is defined as the weighting function and applied to the in-house regression code in this work. The weighting function allows for an equal contribution from any radiance, regardless of data distribution, which is important in the regression analysis.

Appendix B: Derivation of Equation (4)

After simplification with $B(T_{inst}) = B(T_{\mathrm{ICT}})$ and $R_{\mathrm{SV}} = 0$, equation (3) becomes

$$R_{\mathrm{ICT}} = (f_{inst} - \varepsilon_{\mathrm{ICT}} f_{inst} + \varepsilon_{\mathrm{ICT}}) B(T_{\mathrm{ICT}}) + f_{\mathrm{EV}}(1 - \varepsilon_{\mathrm{ICT}}) R_{\mathrm{EV}} \tag{B1}$$

Besides the error caused by ICT BB imperfection effects, another error source is the ICT temperature measurement error, which includes the PRT temperature measurement error, difference between the temperature measured using the embedded PRT and the BB surface temperature, and the BB temperature nonuniformity. These temperature measurement errors can cause a systematic bias and random noise on the calculated ICT radiance. The systematic error is difficult to separate from the BB imperfection effect, and these two effects will be analyzed collectively. In the current L1B calibration algorithm, $R_{ICT\_L1B} = B(T_{\mathrm{ICT}})$, the calibration radiance error becomes

$$\begin{aligned}\Delta R_{\mathrm{ICT}} = R_{\mathrm{ICT\_L1B}} - R_{\mathrm{ICT}} - \left.\frac{dB(T)}{dT}\right|_{T=T_{\mathrm{ICT}}} \Delta T \quad &= R_{\mathrm{ICT\_L1B}} - (f_{inst} - \varepsilon_{\mathrm{ICT}} f_{inst} + \varepsilon_{\mathrm{ICT}}) R_{\mathrm{ICT\_L1B}} \\ &\quad - f_{\mathrm{EV}}(1 - \varepsilon_{\mathrm{ICT}}) R_{\mathrm{EV}} - \left.\frac{dB(T)}{dT}\right|_{T=T_{\mathrm{ICT}}} \Delta T\end{aligned} \tag{B2}$$

A term with $R_{ICT\_L1B} - R_{\mathrm{EV}}$ is used to show the effect of radiance difference between calibration and Earth view. After simplification, equation (B2) becomes

$$\Delta R_{\mathrm{ICT}} = (1 - f_{inst} - f_{\mathrm{EV}})(1 - \varepsilon_{\mathrm{ICT}})R_{\mathrm{ICT\_L1B}} + f_{\mathrm{EV}}(1 - \varepsilon_{\mathrm{ICT}})(R_{\mathrm{ICT\_L1B}} - R_{\mathrm{EV}}) - \left.\frac{\mathrm{d}B(T)}{\mathrm{d}T}\right|_{T=T_{\mathrm{ICT}}} \Delta T \quad \text{(B3)}$$

Dividing by R_{ICT_L1B}, this equation becomes the relative error as expressed in equation (4)

$$\frac{\frac{\Delta R_{\mathrm{ICT}}}{R_{\mathrm{ICT\_L1B}}} = (1 - f_{inst} - f_{\mathrm{EV}})(1 - \varepsilon_{\mathrm{ICT}}) - \frac{1}{R_{\mathrm{ICT\_L1B}}}\left(\frac{\mathrm{d}B(T)}{\mathrm{d}T}\right)_{T=} T_{\mathrm{ICT}}\Delta T_{\mathrm{ICT}} + f_{\mathrm{EV}}(1 - \varepsilon_{\mathrm{ICT}})R_{\mathrm{ICT\_L1B}} - R_{\mathrm{EV}}}{R_{\mathrm{ICT\_L1B}}} \quad \text{(B4)}$$

Acknowledgments

The authors thank Xiong Xiaoxiong, Likun Wang, and Fangfang Yu for discussions on AVHRR and IASI data and sensor thermal band response function This work was supported by the National Oceanic and Atmospheric Administration (NOAA) National Environmental Satellite, Data, and Service (NESDIS) Center for Satellite Applications and Research (STAR) Calibration and Validation fund. Both AVHRR L1B data and IASI L1c data are available for the public and can be downloaded from NOAA CLASS (http://www.class.ncdc.noaa.gov/).

References

Aumann, H. H. and T. S. Pagano (2008), Using AIRS and IASI data to evaluate absolute radiometric accuracy and stability for climate applications, *Atmospheric and Environmental Remote Sensing Data Processing and Utilization IV: Readiness for GEOSS II*, *Int. Soc. Opt. Eng. SPIE Proc.*, Vol. 7085, edited by M. D. Goldberg et al., 8504 pp., SPIE, San Diego, Calif., doi:10.1117/12.795225.

Blumstein, D., et al. (2004), IASI instrument: Technical overview and measured performances, Infrared Spaceborne Remote Sensing XII, *Proc. SPIE*, *5543*, 196–207.

Blumstein, D., B. Tournier, F. R. Cayla, R. F. T. Phupin, C. Bull, and G. Ponce (2007), In-flight performance of the infrared atmospheric sounding interferometer (IASI) on MetOp-A, *Atmospheric and Environmental Remote Sensing Data Processing and Utilization III: Readiness for GEOSS*, *SPIE Proc.*, 6684, 66,840, doi:10.1117/12.560907.

Chang, T., and X. Xiong (2011), Assessment of MODIS thermal emissive bands on-orbit calibration, *IEEE Trans. Geosci. Remote Sens.*, *49*(6), 2415–2425.

Goldberg, M., et al. (2011), The global space-based inter-calibrati on system, *Bull. Am. Meteorol. Soc.*, *92*, 467–475.

Hewison, T. J., X. Wu, F. Yu, Y. Tahara, X. Hu, D. Kim, and M. Koenig (2013), GSICS inter-calibration of infrared channels of geostationary imagers using Metop/IASI, *IEEE Trans. Geosci. Remote Sens.*, *51*, 1160–1170.

Larar, A. M., W. L. Smith, D. K. Zhou, X. Liu, H. Revercomb, J. P. Taylor, S. M. Newman, and P. Schlussel (2010), IASI spectral radiance validation inter-comparisons: Case study assessment from the JAIVEX field campaign, *Atmos. Chem. Phys. Discuss.*, *10*, 411–430.

Madd, E., T. King, H. Sun, W. Wolf, C. Barnet, A. Heidinger, Z. Cheng, and M. Goldberg (2011), Using MetOp-A AVHRR clear-sky measurements to cloud-clear MetOp-A IASI column radiances, *J. Atmos. Oceanic Technol.*, *28*(9), doi:10.1175/JTECH-D-10-05045.1,1104-1116.

Mittaz, J., and A. Harris (2011), A physical method for the calibration of the AVHRR/3 thermal IR channels. Part II: An in-orbit comparison of the AVHRR longwave thermal IR channels on board MetOp-A with IASI, *J. Atmos. Oceanic Technol.*, *28*(9), doi:10.1175/2011JTECHA1517.1,1072-1087.

Mittaz, J., A. Harris, and J. Sullivan (2009), A physical method for the calibration of the AVHRR/3 thermal IR channels 1: The prelaunch calibration data, *J. Atmos. Oceanic Technol.*, *26*, 996–1019.

Ohring, G. (2006), Report of "The Workshop on Achieving Satellite Instrument Calibration for Climate Change (ASIC3)", edited by G. Ohring, Lansdowne, VA., 16–18, May. [Available at http://www.star.nesdis.noaa.gov/star/documents/ASIC3-071218-webversfinal.pdf.]

Phillips, P. L., and P. Schlüssel (2005), Classification of IASI inhomogeneous scenes using co-located AVHRR data, *Proc. SPIE*, *5979*, 597905, doi:10.1117/12.627605.

Press, W. H., S. A. Teukolsky, W. T. Vetterling, and B. P. Flannery (1992), *Numerical Recipes in C*, 2nd ed., pp. 671, Cambridge Univ. Press, Cambridge, U. K.

Steyn-Ross, D. A., and M. L. Steyn-Ross (1992), Radiance calibrations for advanced very high resolution radiometer infrared channels, *J. Geophys. Res.*, *97*(C4), 5551–5568, doi:10.1029/91JC03055.

Sullivan, J. (1999), New radiance-based method for AVHRR thermal channel nonlinearity correction, *Int. J. Remote Sens.*, *20*(18), 3493–3501.

Walton, C., J. Sullivan, C. Rao, and M. Weinreb (1998), Corrections for detector nonlinearities and calibration inconsistencies of the infrared channels of the advanced very high resolution radiometer, *J. Geophys. Res.*, *103*, 3323–3337, doi:10.1029/97JC02018.

Wang, L., and C. Cao (2008), On-orbit calibration assessment of AVHRR longwave channels on MetOp-A using IASI, *IEEE Trans. Geosci. Remote Sens.*, *46*, 4005–4013.

Wang, L., Y. Han, X. Jin, Y. Chen, and D. A. Tremblay (2015), Radiometric consistency assessment of hyperspectral infrared sounders, *Atmos. Meas. Tech.*, *8*, 4831–4844, doi:10.5194/amt-8-4831-2015.

Weinreb, M., G. Hamilton, S. Brown, and R. Koczo (1990), Nonlinearity corrections in calibration of advanced very high resolution radiometer infrared channels, *J. Geophys. Res.*, *95*, 7381–7388, doi:10.1029/JC095iC05p07381.

Xiong, X., K. Chiang, J. Esposito, B. Guenther, and W. L. Barnes (2003), MODIS on-orbit calibration and characterization, *Metrologia*, *40*, 89–92.